J. Quant. Spectrosc. Radiat. Transfer. Vol. 10, pp. 423–448. Pergamon Press 1970. Printed in Great Britain

PHOTOIONIZATION CROSS SECTIONS OF NITROGEN, OXYGEN, CARBON AND ARGON FOR THE SLATER–KLEIN–BRUECKNER POTENTIAL*

G. M. THOMAS and T. M. HELLIWELL†

Jet Propulsion Laboratory, California Institute of Technology, Pasadena, California

(*Received* 10 *October* 1969)

Abstract An approximate central potential model was developed for the calculation of radial wave functions and photoionization cross sections. The model is based on combining the best features of the Slater approximation for the interior of the atom and the Klein–Brueckner approximation for intermediate and large electron radii. The outer subshell radial wave function for the $N(^4S)$ ground state term and the photoionization cross section for the $N(^4S) \rightarrow N^+(^3P)$ transition are compared with Hartree, Hartree–Fock–Slater, quantum defect approximate methods and with detailed Hartree–Fock solutions. Calculations of the photoionization cross sections for nitrogen, oxygen, carbon, and argon are presented for a range of electron energies from threshold to ~ 30 eV. These data are compared with previous theoretical and experimental results. The present method brings the cross sections into close agreement with more detailed methods over the entire frequency range. However, the results do not always agree with experiment, and further improvements will require consideration of electron correlation effects.

1. INTRODUCTION

QUANTITATIVE spectroscopy of high temperature plasmas often requires an accurate calculation of a large number of atomic cross sections for purposes of diagnostics. The quantities of interest include transition probabilities and photoionization cross sections for atoms in various stages of ionization. Recently, there has been considerable interest in the photoionization cross sections of the principal elements making up planetary and terrestrial atmospheres. Measurements of the relevant cross sections have been severely limited because of two experimental difficulties: With the exception of the rare gases, the elements do not exist as free atoms; and for transitions arising from the ground state configuration, the observations must be made in the vacuum ultraviolet spectral region.

Hydrogen-like treatments of atomic photoionization processes are inadequate for the ground state configuration. Quantitative estimates for many-electron atoms rely mainly on the calculation of the relevant matrix elements based on Hartree–Fock wave functions. The HF equations provide the best set of one-electron wave functions in the sense that they are derived from the variational principle. The complexity of the numerical solution of the HF equations has always limited the number of solutions available. This

* This paper presents the results of one phase of research carried out at the Jet Propulsion Laboratory, California Institute of Technology, under Contract No. NAS 7-100, sponsored by the National Aeronautics and Space Administration.

† Harvey Mudd College, Claremont, California.

fact has led to a search for more approximate methods which will allow simplified numerical solutions to be obtained, without a great loss in accuracy in the region of configuration space essential to the calculation.

BURGESS and SEATON[1] have developed the "quantum defect" method based on the use of approximate analytical wave functions for the initial and final states of the system. This method is essentially based on the Coulomb approximation and a normalization factor, depending on experimental ionization energies. The simplest solutions involving SCF wave functions are given by the HARTREE[2] method. Both the "quantum defect" and Hartree methods do not include an allowance for the attractive exchange force.

SLATER[3] introduced the concept of an "average exchange potential" derived from the theory of the free electron gas. The Hartree–Fock–Slater method represents an important simplification of the equations and has been used to advantage in several investigations.[4, 5] However, as pointed out by SLATER,[3] the method breaks down at large electron radii where the central potential does not have the correct asymptotic form. HERMAN and SKILLMAN[5] partially overcame this problem by arbitrarily introducing a cut-off radius for the HFS potential. Beyond the cutoff, the potential reverts to the Coulomb potential. In this approximation the exchange force is neglected at intermediate and large electron radii. As will be shown later, this approximation leads to discrepancies with more exact calculations of the cross section near threshold.

KLEIN and BRUECKNER[6] have recently shown how to analyze the photoionization cross section for negative oxygen ions. The matrix elements for negative ions are strongly dependent on the behavior of the radial wave functions at large electron radii. The method of KB employs a term in the central potential which includes core polarization and implicitly contains an allowance for the exchange force. The polarizability of the atom is treated as a parameter which is adjusted to yield the experimentally observed binding energy for the negative ion. The results of the KB method for the oxygen negative ion were in good agreement with the experimental results of BRANSCOMB.[7] The KB method is semi-empirical in the sense that the polarization forces do not arise naturally in the formulation of the problem. The KB method was originally developed for calculating the elastic scattering of slow electrons off of nitrogen and oxygen atoms. COOPER[8] later employed this method to estimate photodetachment cross sections for several negative ions. KIVEL[9] has extended the KB method to the calculation of Bremmstrahlung cross sections for nitrogen and oxygen.

The present paper describes an improved central potential which is essentially based on a combination of the best features of the HFS and KB methods. The equations describing the photoionization cross sections and approximate central potentials, and the numerical methods for obtaining the solutions are described. The improvements to be expected for wave functions and photoionization cross sections are illustrated by considering several specific examples. Calculations were carried out employing Hartree, Hartree–Fock–Slater, and the present Slater–Klein–Brueckner (SKB) central potentials. We considered several transitions arising from the ground state configuration $1s^2 2s^2 2p^q$ (oxygen, nitrogen and carbon) and one example involving the $1s^2 2s^2 2p^6 3s^2 3p^6$ configuration (argon). These results are compared with existing solutions based on Hartree–Fock wave functions. Comparisons are also made with existing experimental data.

The present work was exploratory in nature. However, the results appear to be sufficiently accurate for many applications. For several of the transitions, it appears that

calculations have not been carried out over the frequency range considered here. In view of this, the photoionization cross sections as a function of photon energy are presented in graphical form in an Appendix of the paper.

II. CALCULATION METHODS

A. *Photoionization cross sections*

The photoionization absorption cross section for a neutral atom in the dipole length formulation is

$$\sigma = \tfrac{4}{3}\pi\alpha a_0^2 \zeta_p (I+\varepsilon)(C_{l-1}M_{l-1}^2 + C_{l+1}M_{l+1}^2) \tag{1}$$

where the matrix elements are given by

$$M_{l'} = \int_0^\infty P(nl;r) r P(\varepsilon l';r)\,\mathrm{d}r \tag{2}$$

$$l' = l \pm 1$$

and the quantity α is the fine structure constant, a_0 is the Bohr radius, I is the ionization energy in Rydbergs, and ε is the electron kinetic energy (also in Rydbergs). The quantities $C_{l\pm1}$ are constants depending on the initial and final states; their values have been tabulated by BATES.[10] The function $P(nl;r)$ is the wave function for the nl bound state, and $P(\varepsilon l';r)$ is the continuum wave function. The constants are chosen in equation (1) to yield cross sections expressed in units of cm^2. The factor ζ_p depends on integrals over the passive electrons and is usually of order unity (cf. BATES[10]). In the present work we will set $\zeta_p = 1$ always. The main problem is to determine the wave functions involved in equation (2).

The radial wave function for the (nl) subshell of the atom is given by

$$\left[\frac{\mathrm{d}^2}{\mathrm{d}r^2} - \varepsilon_{nl} + V(nl;r) - \frac{l(l+1)}{r^2}\right] P(nl;r) = 0 \tag{3}$$

where $P(nl;r)$ is the bound wave function satisfying the normalization

$$\int_0^\infty P^2\,\mathrm{d}r = 1 \tag{4}$$

and boundary conditions

$$P(nl;r) \to 0 \text{ as } r \to \infty$$

$$P(nl;r) \to 0 \text{ as } r \to 0 \tag{5}$$

ε_{nl} is the energy eigenvalue of the (nl) subshell (measured positive for bound states); n and l are the principal and azimuthal quantum numbers, and $V(nl;r)$ is an approximate central potential.

The equations for the free electrons are obtained by replacing ε_{nl} by $-\varepsilon$, the electron kinetic energy, and replacing l by $l' = l \pm 1$, i.e.

$$\left[\frac{\mathrm{d}^2}{\mathrm{d}r^2} + \varepsilon + V(nl;r) - \frac{l'(l'+1)}{r^2}\right] P(\varepsilon l';r) = 0. \tag{6}$$

The free waves are normalized numerically at large r (cf. BATES and SEATON[11]), where they approach $\varepsilon^{-1/4}$. The quantity $V(nl;r)$ is assumed to be the same effective central potential used in equation (3).

The assumptions that the bound and free electrons move under the same effective central potential, and that the overlap factor ζ_p for the passive electrons equals unity, implies that the ionic core is unrelaxed. The rationale for this model has been discussed in detail by COOPER.[12] In particular, the dipole length, velocity, and acceleration matrix elements are identical for the unrelaxed core model.

B. *Approximate central potentials*

The central potential in equation (3) depends on integrals over all of the (nl) orbitals of the atom. Hartree's potential, which ignores the exchange forces, may be written

$$\mathrm{HAR}(r) = -\frac{2Z}{r} + \frac{2}{r}\sum_{n'l'} \omega(n'l')Y_0(n'l';r) \tag{7}$$

the first term on the right hand side of equation (7) is the nuclear coulomb potential for a neutral atom of atomic number Z, and the second term is the electron coulomb potential. The quantity $\omega(n'l')$ is the number of occupied wave functions in the (nl) subshell and $Y_0(nl;r)$ is the integral

$$Y_0(nl;r) = \int_0^r P^2(nl;t)\,\mathrm{d}t + r\int_r^\infty \frac{P^2(nl;t)}{t}\,\mathrm{d}t. \tag{8}$$

In equation (7), the sum is over all (nl) except the one being calculated. Thus, equation (3) is only one of a set of coupled integro-differential equations which must be solved simultaneously in order to evaluate the potential. The central potential is different for each (nl) subshell and does not include the effects of exchange or polarization.

Equation (3) may be solved by an iterative numerical technique to be described later. Since the equation is homogeneous, the solutions may be carried out in two parts: first, finding solutions of equation (3) satisfying the conditions (5), and later on normalizing these solutions. The Hartree–Fock equations, in contrast, contain additional exchange terms $X(nl;r)$ on the right hand side of equation (3) which considerably increase the labor involved in obtaining the numerical solutions, since the equations are then inhomogeneous. This complication arises because the normalization condition, equation (4), must be satisfied simultaneously with the boundary conditions at each stage of the calculation for each (nl).

SLATER[3] introduced an important simplifying assumption derived from the theory of the free electron gas for treating the exchange term. He introduced the concept of an average exchange potential $V_{\mathrm{ex}}(r)$ which replaces the integral terms involved in evaluating the exchange integrals $X(nl;r)$. The function $V_{\mathrm{ex}}(r)$ is the same function of r for all (nl) subshells and is given by

$$V_{\mathrm{ex}}(r) = -6\left[\frac{3}{32\pi^2}\frac{\sum_{nl}\omega(nl)P^2(nl;r)}{r^2}\right]^{1/3}. \tag{9}$$

The Hartree–Fock–Slater potential is then given by

$$\mathrm{HFS}(r) = V^*_{\mathrm{coul}} + V_{\mathrm{ex}} \tag{10}$$

where

$$V^*_{\mathrm{coul}} = -\frac{2Z}{r} + \frac{2}{r}\sum_{nl} Y_0(nl; r) \tag{11}$$

is the modified coulomb potential consistent with the Slater approximation. The sums in equations (9) and (11) are over all (nl) subshells and do not exclude the orbital being calculated. The function V^*_{coul} approaches zero at large r, whereas the correct coulomb potential V_{coul} defined by equation (7) asymptotically approaches $-2/r$ as $r \to \infty$. This fact leads to inaccurate results for the potential at even intermediate values of r.

HERMAN and SKILLMAN[5] attempted to overcome this problem by introducing a cutoff radius r_0 for the HFS potential such that

$$\begin{aligned} V(r) &= \mathrm{HFS}(r) \qquad r < r_0 \\ V(r) &= \frac{-2}{r} \qquad r \geq r_0 \end{aligned} \tag{12}$$

where r_0 is the value of r satisfying

$$\mathrm{HFS}(r_0) = \frac{-2}{r_0}.$$

This modification assures that the correct asymptotic form is obtained at large r at the expense of not including the exchange force at intermediate and large values of r. The above approximation was employed in our HFS calculations.

For the calculation of photoionization cross sections at low electron energies near threshold the approximation equation (12) can lead to discrepancies with the Hartree–Fock results. We have attempted to obtain an improved central potential by extending the method developed by Klein and Brueckner. The method of KB introduces a polarization potential

$$V_{\mathrm{pol}} = \frac{-p}{(r^2 + r_p^2)^2} \tag{13}$$

where p is the average polarizibility and is the same for all (nl). The quantity r_p is an adjustable parameter which is approximately equal to the average electron radius $\bar{r}$ for the outer (nl) orbital. For negative ions, the polarizability is adjusted to yield the correct binding energy for the negative ion. The polarization potential as defined in equation (13) also implicitly contains an allowance for the shorter range exchange potential. We have taken advantage of this fact in the present study. We construct a new central potential defined as follows:

$$\begin{aligned} V_i(r) &= \mathrm{HFS}(r) \qquad r < r_m \\ V_0(r) &= V_{\mathrm{coul}} + V_{\mathrm{pol}} \qquad r \geq r_m \end{aligned} \tag{14}$$

where r_m is the matching radius where we join the inner and outer solutions and r_m is the value of r satisfying

$$V_I(r_m) = V_O(r_m).$$

For the ground states of neutral atoms with large binding energies, the polarization effects at large radii are expected to be small. However, the approximate inclusion of exchange in V_{pol} will have a marked effect on the "valence" electron wave functions at intermediate and large values of r. In this approximation, the set of simultaneous equations to be solved are of the form given by equation (3) and may be solved in as simple and straightforward a manner as the Hartree equations.

C. *Numerical methods*

Equation (3) must be solved simultaneously for all (nl) subshells. In performing the numerical integration of this set of equations it is convenient to introduce the auxiliary variable (cf. HARTREE[2]),

$$y = P' - \frac{(l+1)}{r} P. \tag{15}$$

Equations (15) and (3) then yield the following equation

$$y' = [\varepsilon_{nl} - V(r)]P - \frac{(l+1)y}{r}. \tag{16}$$

Equations (15) and (16) are two first order differential equations which now replace equation (3). The two equations were solved simultaneously using a predictor-corrector scheme. The predictor-corrector method has the advantage that errors do not grow, i.e. the integration has absolute stability if the proper step size is chosen. It has the further advantage that an estimate of the truncation error flows smoothly out of the computation, and corrections for this error may be applied during the calculations.

The general method of solution of the set of difference equations is as follows:

1. Trial functions $P(nl; r)$ are used to calculate a trial potential $V(nl; r)$.
2. Initial guesses of the energy eigenvalues ε_{nl} are made.
3. The equations are integrated out from the origin and will not satisfy the boundary conditions, equation (5).
4. The energy eigenvalues are adjusted until values are found which satisfy the boundary conditions.
5. The functions are normalized.
6. The new set of wave functions are used to calculate an improved central potential and the entire process is replaced until successive iterations converge.

In using this technique the computation time is considerably reduced by employing good initial estimates of the trial functions. The method which we have employed is to use the Thomas–Fermi statistical model for the initial estimates. An analytical fit to this potential has been given by LATTER[13] and was employed in the present calculations.

The inner boundary condition $P(0) = 0$ was automatically satisfied in the calculations by employing the power series expansion of $P(nl; r)$ valid for small r as given by HARTREE.[2] The expansion also provided starting values for the numerical integration of the differential equations.

The outer boundary condition $P \to 0$ as $r \to \infty$ requires the improvement of the initial guesses for the energy eigenvalues by a convergence procedure. The method adopted depends upon the establishment of upper and lower bounds for the energy eigenvalue. These bounds are established by requiring that the wave function have exactly $n-l-1$ nodes and in addition that the function approaches zero beyond the last node. In successive adjustments of the energy the upper and lower bounds were made to approach each other by decreasing the energy increment until the wave functions differed from zero by only a small prescribed amount.

The problem of stability of the iterative solution deserves mention. If one uses the output wave functions of one stage of the iteration as the input for the succeeding stage, the solutions often diverge. In place of step (6) above, we used a simple arithmetic average of the input and output wave functions for calculating the trial potential. This method was observed to be stable in all cases treated in the present paper.

For numerical accuracy, the computer code allows the selection of four different increments of step size in the predictor-corrector method. The step size was as small as $h = 0.001$ in the region near the origin and was increased at prescribed values of r until a final value $h = 0.08$ was employed at large electron radii where the function varies slowly with r. Calculations were carried out over the range in $s = r/\bar{r}$ from 0.001 to 14.

The iterative process was considered to have converged when the energy eigenvalues were within 0.01 per cent of the values from the preceding stage of iteration for all (nl) subshells. Convergence of the eigenvalues was very rapid, typically, the values were within one per cent of the final values after three or four cycles of the iteration. An additional four or five cycles were required to obtain final convergence to 0.01 per cent.

Once the self consistent potential for the neutral atom is obtained, the same potential is used in equation (6) to calculate the free wave functions. For normalization of the continuum functions we employed the method described by BATES and SEATON.[11] This method requires that the asymptotic amplitude of the wave function approaches $\varepsilon^{-1/4}$ at large electron radius. No iterations are required for the free waves. The calculations were done for electron energies ranging from 0 to ~ 30eV. Having the free and bound wave functions, the matrix elements were evaluated using Simpson's rule.

D. *Input data*

The values of p and r_p used in the calculations are listed in Table 1. The cut-off parameter r_p was set equal to the mean radius $\bar{r}$ of the "valence" electron. The values of $\bar{r}$ were taken from the HF results listed in HARTREE's[2] book. For nitrogen and oxygen the experimental polarizability values of ALPHER and WHITE[14] were adopted. The theoretical value of p obtained by COOPER[8] was employed for the carbon atom. For argon we employed the following theoretical scaling law

$$p = \text{Const}\, Z r_p^4. \tag{17}$$

This relation was used by KB to predict the polarizability of nitrogen using the theoretically derived values for oxygen. The constant in equation (14) was evaluated using COOPER's[8] theoretical results for Cl which were: $p = 23.26$. Since Cl has $Z = 17$ and argon has an atomic number 18, the Z scaling is small. The valence electron for Cl has an average radius $\bar{r} = 2$. Using equation (17) the extrapolated polarizability obtained for argon was $p = 10.6$

TABLE 1. MEAN RADIUS OF THE ACTIVE ELECTRON, $\bar{r} = \int_0^\infty rP^2\,dr$, AND THE AVERAGE POLARIZABILITY, p, USED IN THE SKB CALCULATIONS

Element	$\bar{r}$	p
N	1.414[a]	7.6[b]
O	1.20[a]	5.2[b]
C	1.71[a]	17.5[c]
A	1.66[a]	10.6[d]

[a] HARTREE.[2]
[b] ALPHER and WHITE.[14]
[c] COOPER.[8]
[d] Theoretically scaled from CI results of COOPER.[8]

atomic units. The results of the calculations for argon showed that the cross sections are only weakly dependent on the value of p, and no further efforts were made to improve on the extrapolated value.

All of the transitions corresponding to ejection of an outer $2p^q$ electron (N, O, C) or a $3p^q$ electron (argon) are listed in Table 2. Thus, only those transitions leaving the active electron in the final states εs or εd are involved in the dipole length matrix elements. The values of the transition probabilities C_s (cf. BATES[10]) and the experimental ionization

TABLE 2. TRANSITION PROBABILITY, C_s, AND IONIZATION ENERGIES, I, USED IN EQUATION (1) FOR EJECTION OF OUTER $2p^q$ ELECTRONS FOR NITROGEN, OXYGEN AND CARBON

Element	(Initial → Final)	C_s[a]	I[b] (Ry)
N	$p^3(^4S) \rightarrow p^2(^3P)$	1	1.069
N	$p^3(^2D) \rightarrow p^2(^3P)$	$\frac{1}{2}$	0.894
	$p^3(^2D) \rightarrow p^2(^1D)$	$\frac{1}{2}$	1.034
N	$p^3(^2P) \rightarrow p^2(^3P)$	$\frac{1}{2}$	0.807
	$p^3(^2P) \rightarrow p^2(^1D)$	$\frac{5}{18}$	0.946
	$p^3(^2P) \rightarrow p^2(^1S)$	$\frac{2}{9}$	1.104
C	$p^2(^3P) \rightarrow p(^2P)$	$\frac{2}{3}$	0.828
C	$p^2(^1D) \rightarrow p(^2P)$	$\frac{2}{3}$	0.735
C	$p^2(^1S) \rightarrow p(^2P)$	$\frac{2}{3}$	0.631
O	$p^4(^3P) \rightarrow p^3(^4S)$	$\frac{4}{9}$	1.001
	$p^4(^3P) \rightarrow p^3(^2D)$	$\frac{5}{9}$	1.245
	$p^4(^3P) \rightarrow p^3(^2P)$	$\frac{1}{3}$	1.370
O	$p^4(^1D) \rightarrow p^3(^2D)$	1	0.856
	$p^4(^1D) \rightarrow p^3(^2P)$	$\frac{1}{3}$	1.225
O	$p^4(^1S) \rightarrow p^3(^2P)$	$\frac{4}{3}$	0.693
A	$p^6(^1S) \rightarrow p^5(^2P)$	2	1.158

[a] BATES.[10]
[b] MOORE.[15]

energies I (Rydbergs) from MOORE[15] are also listed in Table 2. The coefficients C_d are always given by $C_d = 2C_s$.

In the present approximation the bound wave function $P(nl; r)$ and the free wave function $P(\varepsilon l; r)$ are assumed to be same for all of the transitions in a given atom. The cross section results for the individual transitions listed in Table 2 differ only through their dependence on the $C_{l\pm1}$ coefficients and the different ionization energies as given by equation (1).

III. RESULTS

A. *Comparison of approximate solutions*

The general behavior of the radial wave functions under various potentials may be illustrated by considering the transition

$$N(1s^2 2s^2 2p^3)^4S + h\nu \rightarrow N^+(1s^2 2s^2 2p^2)^3P + e^- \tag{18}$$

which is representative of the general behavior to be expected of transitions involving the ejection of an outer $2p^q$ electron. For the purpose of comparing the radial wave functions, we define the fractional difference

$$\frac{\Delta P}{P} = \frac{P_x}{P} - 1$$

where P_x is the radial wave function for a given central potential and P is the corresponding Hartree–Fock function tabulated by HARTREE.[2]

The results for the $N(^4S)$ transition are presented in Fig. 1. Three curves are shown representing the results for the Hartree, Hartree–Fock–Slater, and the Slater–Klein–Brueckner (SKB) potentials. The normalized electron radius, $s = r/\bar{r}$, covers the range from 0 to 5 in Fig. 1.

The following remarks may be made about Fig. 1:

(1) At small electron radii the Hartree wave function is too small, while the corresponding solutions for the HFS and SKB potentials are too large. This follows from the fact that the Hartree potential does not include the attractive exchange force, while the Slater approximation overestimates the exchange term. The agreement could be improved by introducing empirical factors for reducing the exchange force, however this was not done since the dipole length matrix elements are not affected much by the behavior at small radii.

(2) At large electron radii the Hartree function is too large and in fact becomes divergent. The HFS function, having the same asymptotic potential, also diverges but the divergence occurs at larger radius. The SKB function, on the other hand, is slightly negative over most of the range and remains within about 10 per cent of the Hartree–Fock values.

In Fig. 2 we present the photoionization cross section results for the transition of equation (18) as a function of photon energy (Rydbergs). The cross section is in megabarn units ($1\ M_b = 10^{-18}\ \text{cm}^2$) and is presented for energies ranging from threshold to 7 Rydbergs. The three curves represent results obtained using Hartree (circles), HFS (squares), and SKB (triangles) potentials. HAHNE[16] has used the quantum defect method of Burgess and Seaton to estimate the cross section for this transition. His results are shown as the crosses in Fig. 2.

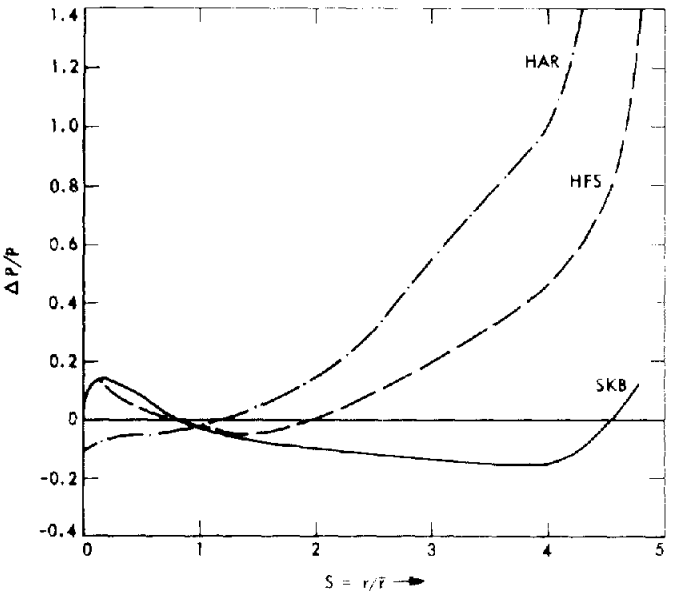

FIG. 1. Fractional deviations, $\Delta P/P$, of the approximate radial wave functions from the Hartree–Fock values of HARTREE,[2] as a function of the normalized electron radius, $s = r/\bar{r}$. Results are for the transition described by equation (18). Curve HAR, Hartree potential; Curve HFS, Hartree–Fock–Slater potential; and curve SKB, Slater–Klein–Brueckner potential, present paper.

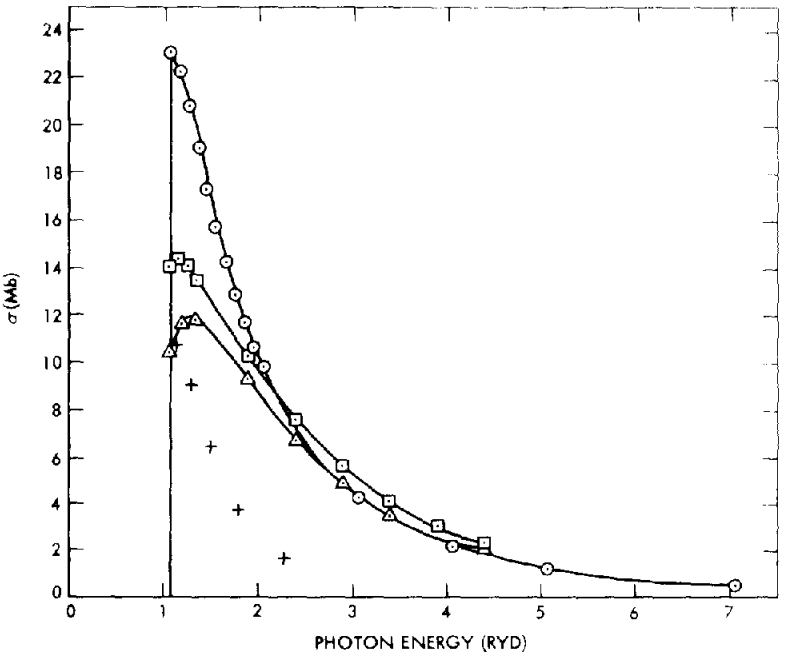

FIG. 2. Photoionization cross section of atomic nitrogen for the transition of equation (18). ○ Hartree potential; □ Hartree–Fock–Slater; △ Slater–Klein–Brueckner (SKB), present paper; and + quantum defect method, HAHNE.[16]

The major contribution to the cross section results from the $2p \rightarrow \varepsilon d$ transition. The d wave is entirely dominated by the centrifugal potential term, and therefore is not significantly affected by the form of the potential. As a result, the principal differences in the results of Fig. 2 are determined by the behavior of the bound wave function. The threshold cross sections are strongly dependent on the form of the potential. The highest cross section values are for the Hartree potential. The inclusion of the Slater exchange force in the potential results in a large decrease in the cross section. The net effect of increasing the attractive potential by adding an additional polarization and exchange force is to further decrease the cross section in the SKB approximation.

The energy dependence of the cross section is a measure of the balance between the centrifugal potential and the energy of the ejected electron. As the electron energy increases, the free waves move in toward the origin. For the HFS and SKB cross-sections this causes, first, an increase as the region of maximum density of the free wave penetrates the high density region of the bound wave, and then a decrease as the negative portion of the d wave moves in to cause cancellation. At high electron energies the free wave is dominated by the electron energy and is nearly independent of the form of the potential (Born approximation). As a result, all of the solutions merge as the photon energy increases.

The quantum defect method is based essentially on a coulomb potential and a normalization of the bound wave function to the experimental binding energy—This approximation agrees with the SKB method at threshold, however, the cross section falls off too rapidly with increasing photon energy.

A summary of the energy eigenvalues for all (nl) orbitals of nitrogen, oxygen, and carbon is presented in Table 3. The column labelled HER represents the energy eigenvalues of HERMAN and SKILLMAN[5] obtained using the Hartree–Fock–Slater method. Comparison with the present HFS calculations in the next column shows that the difference of the energy values is less than one per cent, and may be regarded as a measure of the numerical accuracy involved in the two independent calculations. The next two columns give the results for the SKB and Hartree methods. For the "valence electrons" the SKB energies, are higher than the ionization energies listed by Moore. The Hartree and HFS results are always lower than the observed ionization energies. However, for the innermost (1s) electron, the pattern reverses, i.e., the Hartree results are higher than the other solutions.

TABLE 3. ENERGY EIGENVALUES, ε_{nl}, OBTAINED USING SEVERAL DIFFERENT CENTRAL POTENTIALS. COLUMN HER, HFS POTENTIAL, HERMAN AND SKILLMAN;[5] COLUMN HFS, HFS POTENTIAL, THIS PAPER; COLUMN SKB, SKB POTENTIAL, THIS PAPER; COLUMN HAR, HARTREE POTENTIAL, THIS PAPER

Atom	Orbital, nl	HER	HFS	SKB	HAR
C	1s	21.378	21.503	21.223	22.837
N	1s	29.737	29.726	29.653	31.660
O	1s	39.456	39.428	39.195	41.642
C	2s	1.290	1.302	1.728	1.210
N	2s	1.696	1.707	1.989	1.577
O	2s	2.144	2.147	2.451	1.963
C	2p	0.660	0.668	1.083	0.609
N	2p	0.845	0.851	1.123	0.767
O	2p	1.041	1.044	1.343	0.919

The SKB energy eigenvalues for argon are presented in Table 4. For comparison, the Hartree–Fock energies of HARTREE and HARTREE[17] are also presented. The SKB results are again larger for the valence electron and less than the Hartree–Fock energies for all inner shell electrons.

TABLE 4. ENERGY EIGENVALUES, ε_{nl}, FOR ARGON. COLUMN HH, HARTREE AND HARTREE;[17] COLUMN SKB, THIS PAPER

Orbital, nl	HH	SKB
1s	237.2	230.5
2s	24.6	23.0
2p	19.1	18.3
3s	2.56	2.31
3p	1.18	1.24

B. *Comparison with other work*

Experimental and theoretical results were not available for comparison with all of the transitions listed in Table 2. The following discussion will concern only selected transitions which have been studied in other investigations. The remainder of the results are presented in graphical form as the sum of all transitions from a given initial configuration to all final states of the residual ion in Appendix A.

In Fig. 3 we present the photoionization cross sections for the $N(^4S)$ transition of equation (18). The solid line represents the present calculations as a function of wavelength from threshold to 200 Å. COMES and ELZER[18] have recently measured this cross section using a crossed-beam technique. Their data is shown as the circles in Fig. 3. In comparing the data with the calculations it should be noted that we have not included the contribution corresponding to the ejection of the inner shell (2s) electron by the transition

$$N(1s^2 2s^2 2p^3)^4S + h\nu \rightarrow N^+(1s^2 2s 2p^3)^5S, {}^3S + e^- \tag{19}$$

which has a threshold at 610 Å. Furthermore, we do not include discrete transitions. CARROLL *et al.*[19] have observed a new Rydberg series in the spectral region 694–612 Å. They have attributed this spectrum to transitions arising from the ^4S ground state of nitrogen and ending in the Rydberg terms $2s2p^3(^5S)np\ ^4P$. These spectral features are apparent in Fig. 3 and are not included in the present calculations. With the exception of the line structure, the data are in good agreement with the SKB results from threshold to approximately 500 Å. In the vicinity of threshold the present results are approximately 5 per cent higher than the experimental data.

SAMSON and CAIRNS[20] have measured the molecular nitrogen absorption cross sections in this spectral region using an ion counting technique. The squares plotted in Fig. 3 represent one-half of the molecular nitrogen cross sections. This type of comparison has previously been employed by HENRY.[21] The molecular data in this form are seen to agree both in slope and magnitude with the present cross sections for wavelengths shorter than 400 Å.

As already pointed out, the present model ignores coupling between final states and the effects of core relaxation. HENRY and LIPSKY[22] have recently derived expressions which

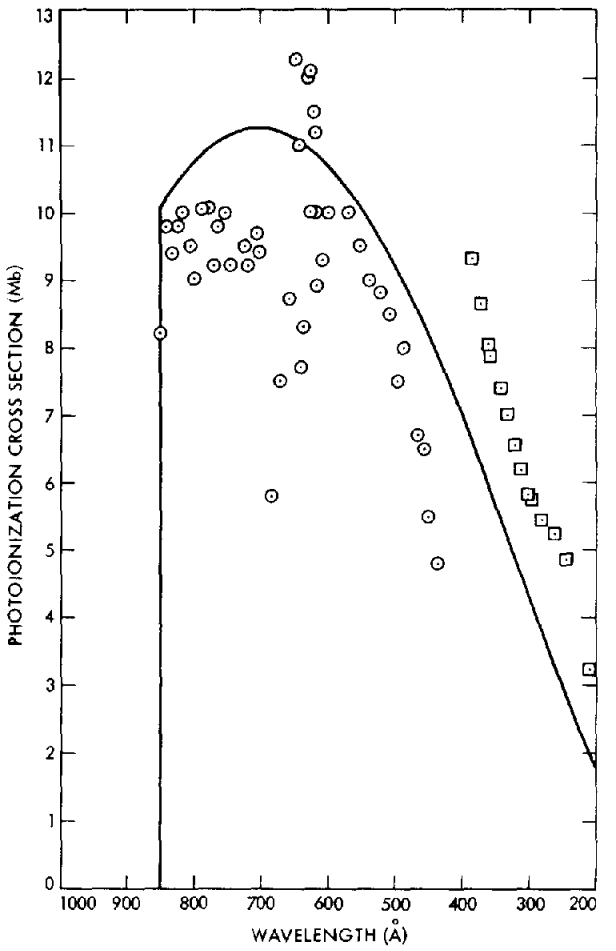

FIG. 3. Photoionization cross section of atomic nitrogen for the transition of equation (18). The Solid Curve represents the present (SKB) results. The circles represent the experimental results of COMES and ELZER[18] and the squares denote one-half of the experimental molecular nitrogen cross section results of SAMSON and CAIRNS.[20]

do not include these two assumptions. They found that the coupling terms had little effect on the total cross section for the specific case of neon. Their formulation of the problem did result in obtaining improved agreement between length and velocity formulated cross sections near the spectral head. HENRY[21] has applied these so called "multi-channel" expressions to the calculation of the photoionization cross sections for atomic nitrogen. His results also include the ejection of the inner shell (2*s*) electron mentioned earlier.

Figure 4 presents a comparison with Henry's results calculated in the length and velocity formulations. The present dipole length cross sections are shown as the solid curve and the dashed curves represent the "multi-channel" estimates. Near threshold, our results agree with the length values both in magnitude and slope. At shorter wavelengths our calculation agrees best with the velocity cross sections. It is difficult to say which of the formulations is

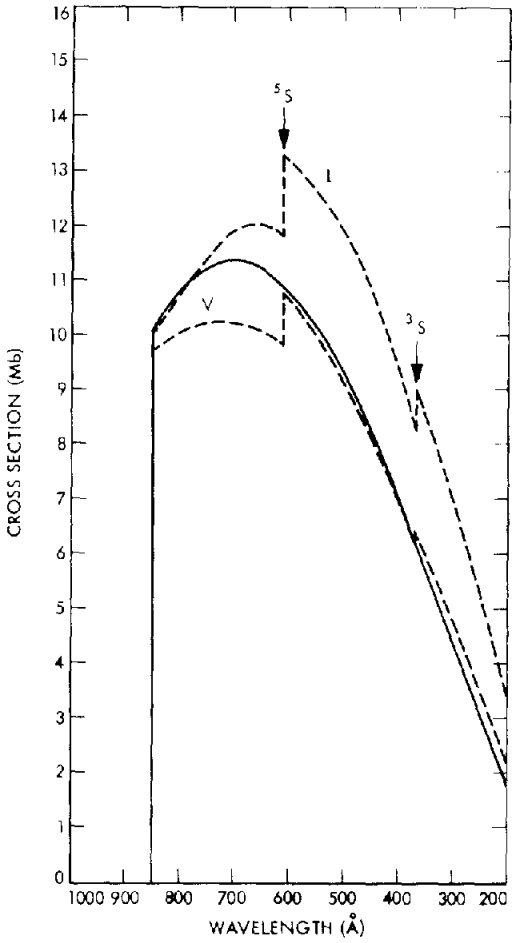

FIG. 4. Photoionization cross section of atomic nitrogen for the transition of equation (18). Solid curve same as in Fig. 3. The results are compared with the calculations of HENRY[21] which are shown as the two dashed curves. The dashed curve labeled L denotes dipole length results and the one labeled V represents the velocity formulation results.

the more accurate. Henry attributes the differences in the two formulations to correlation effects and/or the neglect of core polarization.

DALGARNO, HENRY and STEWART[23] have calculated the photoionization cross sections of atomic oxygen. Hartree–Fock wave functions were employed using length and velocity formulations for the cross section. In Fig. 5 our results for the sum of the transitions

$$O(1s^2 2s^2 2p^4)^3P + h\nu \rightarrow O^+(1s^2 2s^2 2p^3)^4S, 2D, {}^2P + e^- \tag{20}$$

are shown as the solid line. These transitions are important for studies of the formation of the ionosphere. Dalgarno's velocity results at the location of several prominent solar lines are shown as the circles in Fig. 5. He considers the velocity values to be the more accurate of the two formulations. For wavelengths shorter than approximately 650 Å our results are in excellent agreement with the velocity cross sections. His values tend to

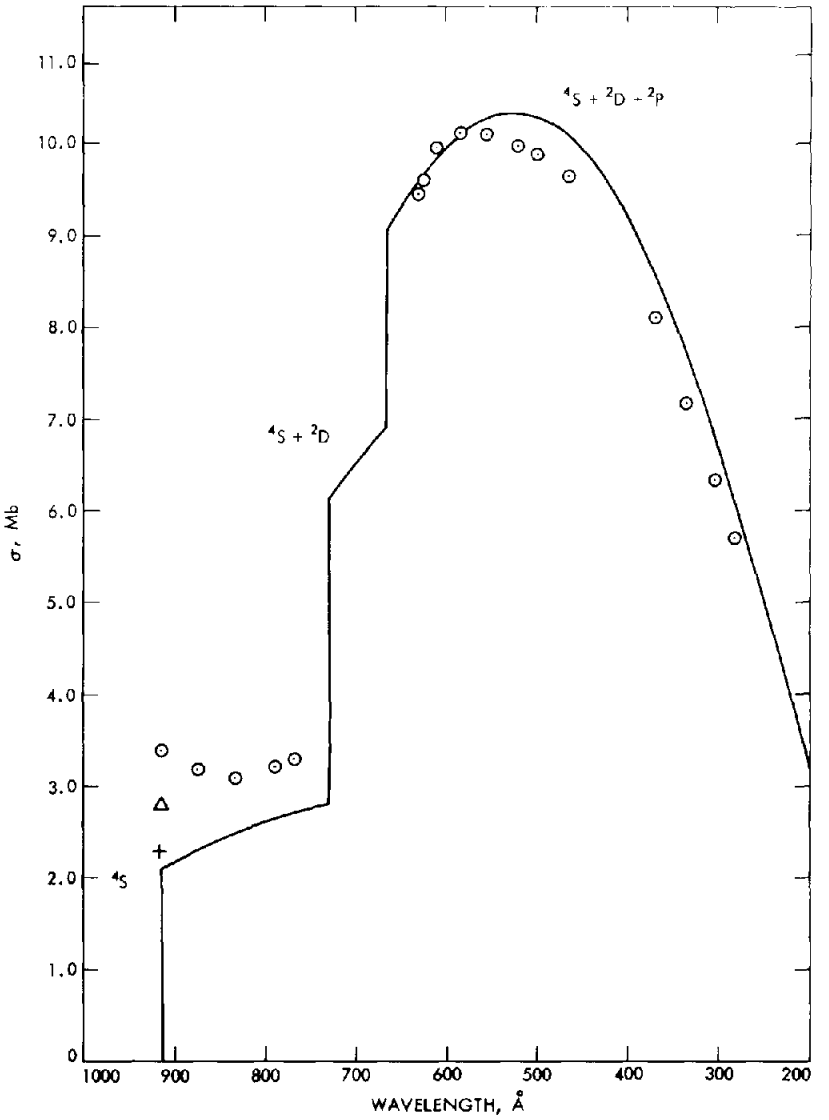

FIG. 5. Photoionization cross section of atomic oxygen for the sum of the transitions described by equation (20). There are three thresholds corresponding to the final states ^4S, ^2D and ^2P of the residual ion. The solid line represents the present SKB results. Circles represent velocity results of DALGARNO *et al.*,[23] and triangles and crosses represent the BATES and SEATON[11] length and velocity results, respectively.

lie higher than the present calculations in the vicinity of the spectral head. The dipole length approximation values of BATES and SEATON[11] shown in Fig. 5 are in better agreement with the present results. Their dipole velocity approximation is 25 per cent lower than the corresponding estimates of Dalgarno.

BATES and SEATON[11] have calculated the photoionization cross sections of carbon, oxygen, and nitrogen using dipole length and velocity formulations. Their results for shorter wavelengths were obtained using more approximate methods. In Table 5 we present a comparison of the results of DALGARNO *et al.*,[23] BATES and SEATON,[11] and the present results at the spectral head for N, O, and C. For oxygen, Dalgarno's values are approxi-

TABLE 5. PHOTOIONIZATION CROSS SECTIONS AT THE SPECTRAL HEAD FOR NITROGEN, OXYGEN AND CARBON. CROSS SECTIONS ARE IN MEGABARNS. THE LETTERS L AND V DESIGNATE THE DIPOLE LENGTH AND DIPOLE VELOCITY FORMULATIONS, RESPECTIVELY. COLUMN BS, BATES AND SEATON;[11] COLUMN DHS, DALGARNO, HENRY AND STEWART;[23] COLUMN SKB, THIS PAPER

Atom	BS		DHS		SKB
	L	V	L	V	L
N	10.2	7.7	...	...	10.1
C	12.5	9.0	...	...	9.3
O	2.3	2.8	2.7	3.4	2.1

mately 25 per cent higher than Bates and Seaton in both formulations. Our results for oxygen and nitrogen are within 10 per cent of the Bates and Seaton length values. However, for carbon the present results tend to agree better with the velocity results of Bates and Seaton. Since both of these investigators employed Hartree–Fock wave functions, it is difficult to say which of the results are the more accurate.

In Fig. 6 we consider the transition described by equation (20) for the spectral region from 600 to 150 Å. The circles in the figure represent one-half the molecular oxygen cross section measured by SAMSON and CAIRNS.[20] The agreement with the calculation is remarkably good. This agreement may be somewhat fortuitous, considering the differences in structure between molecules and atoms.

Photoionization cross sections for argon in the spectral range from threshold to 250 Å are presented in Fig. 7 for the transition

$$A(1s^2 2s^2 2p^6 3s^2 3p^6)^1S + h\nu \rightarrow A^+(1s^2 2s^2 2p^6 3s^2 3p^5), ^2P + e^-. \tag{21}$$

COOPER[12] in his investigation of several of the rare gases has employed Hartree–Fock wave functions to calculate the cross section for this transition. His results are shown as the squares in Fig. 7. Experimental measurements of the argon photoionization cross section have been made by SAMSON and KELLEY[24] using an ion counting technique. Their data is shown as the circles in Fig. 7. The two calculations are seen to agree both in magnitude and slope. However, the calculations are in poor agreement with the experimental data. COOPER[12] has attributed this lack of agreement to the neglect of correlation effects in the central field theory.

IV. CONCLUSIONS

A central field model was defined and used to obtain radial wave functions and photoionization cross sections which are in good agreement with detailed Hartree–Fock results. On the basis of a comparison with HF solutions this method appears to agree with results

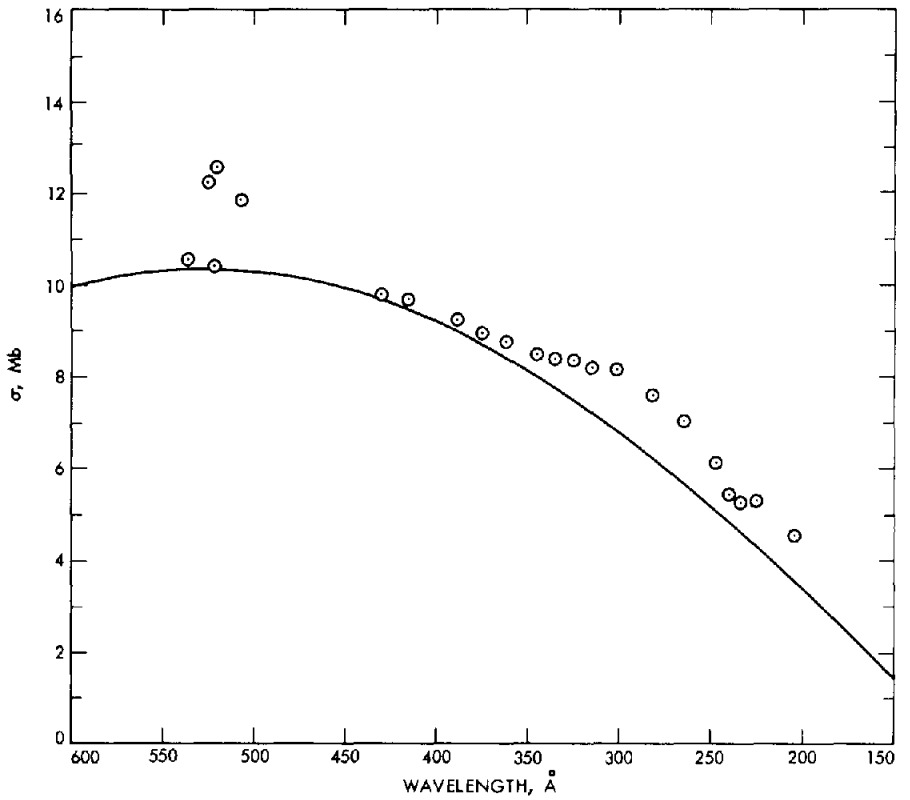

FIG. 6. Photoionization cross section of atomic oxygen for the sum of the transitions described by equation (20). Solid curve as in Fig. 5. Circles represent the $1/2\sigma(O_2)$ experimental results of SAMSON and CAIRNS.[20]

obtained using the dipole length formalism near the spectral head. At higher photon energies the solution approaches dipole-velocity cross section results. For nitrogen, the cross sections are in good agreement with the experimental data of COMES and ELZER.[18] The results for argon are in agreement with COOPER'S[12] HF solutions; however, the theoretical results are in poor agreement with the experimental data of Samson. This discrepancy is probably due to the lack of inclusion of correlation effects. The extension of this model to calculations of photoionization cross sections and transition probabilities for ionized atoms appears to be feasible.

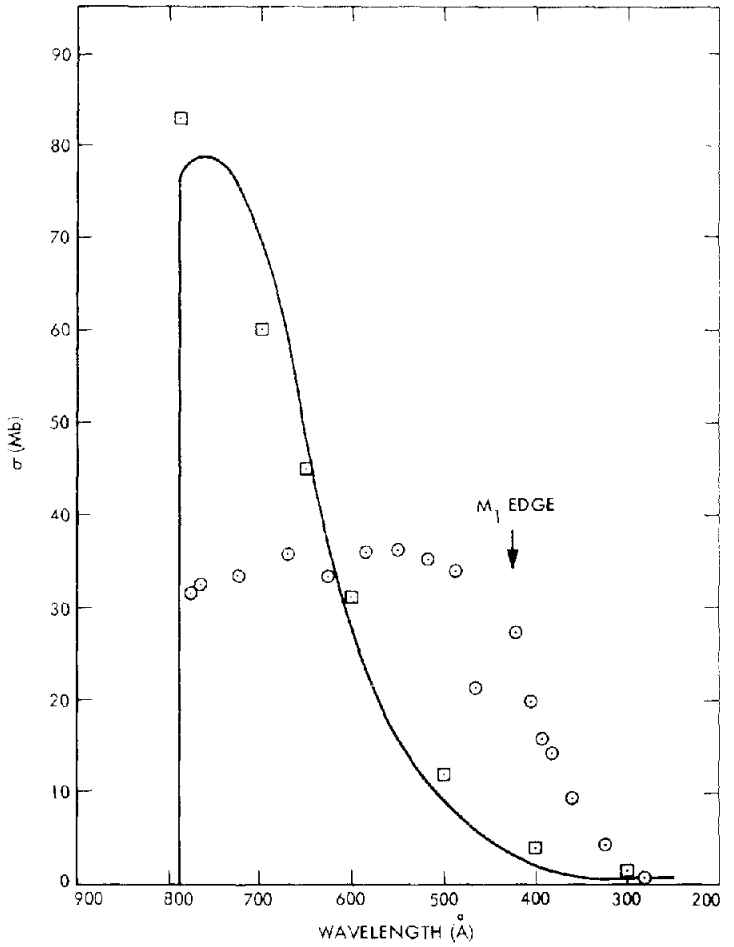

FIG. 7. Photoionization cross section for the atomic argon transition described by equation (21). Solid line, SKB results, present paper. Squares represent Hartree Fock, unrelaxed core results of COOPER.[12] Circles are the experimental results of SAMSON and KELLEY.[24]

REFERENCES

1. A. BURGESS and M. J. SEATON, *Rev. Mod. Phys.* **30,** No. 3 (1958).
2. D. R. HARTREE, *The Calculation of Atomic Structures*, John Wiley, New York (1957).
3. J. C. SLATER, *Phys. Rev.* **81,** No. 3, 385 (1951).
4. P. S. KELLEY, *JQSRT* **4,** 117 (1964).
5. F. HERMAN and S. SKILLMAN, *Atomic Structure Calculations*, Prentice-Hall, Englewood Cliffs, New Jersey (1963).
6. M. M. KLEIN and K. A. BRUECKNER, *Phys. Rev.* **111,** 1115 (1958).
7. I. BRANSCOMB, D. BURCH, S. SMITH and S. GELTMAN, *Phys. Rev.* **111,** 505 (1958).
8. J. W. COOPER, *Phys. Rev.* **126,** 1482 (1962).
9. B. KIVEL, *JQSRT* **7,** 27 (1967).
10. D. R. BATES, *Mon. Not. R. Astr. Soc.* **106,** 432 (1946).
11. D. R. BATES and M. J. SEATON, *Mon. Not. R. Astr. Soc.* **109,** 698 (1949).
12. J. W. COOPER, *Phys. Rev.* **128,** 681 (1962).

13. R. LATTER, *Phys. Rev.* **99,** No. 2, 510 (1955).
14. R. A. ALPHER and D. R. WHITE, *Phys. Fluids* **2,** 153 (1959).
15. C. E. MOORE, *Atomic Energy Levels*, Vol. I, NBS Circular 467 (1949).
16. G. E. HAHNE, NASA TN D-2794, Ames Research Center, Moffet Field, California (1965).
17. D. R. HARTREE and W. HARTREE, *Proc. Roy. Soc. (Lond.)*, Series A, **166,** 450 (1938).
18. F. J. COMES and A. ELZER, *Z. Naturforsch* **23A,** 133 (1968).
19. P. K. CARROLL, R. E. HUFFMAN, J. C. LARRABEE and Y. TANAKA, *Astrophys. J.* **146,** 553 (1966).
20. J. A. R. SAMSON and R. B. CAIRNS, *J. Opt. Soc. Am.* **55,** 1035 (1965).
21. R. J. W. HENRY, *J. Chem. Phys.* **48,** 3635 (1968).
22. R. J. W. HENRY and L. LIPSKY, *Phys. Rev.* **153,** 51 (1967).
23. A. DALGARNO, R. J. W. HENRY and A. L. STEWART, *Planet Space. Sci.* **12,** 235 (1964).
24. J. A. R. SAMSON and F. L. KELLEY, NASA Contractor Report NASA CR-68, Geophysics Corp. of America, Washington, D.C. (1964).

APPENDIX A

The following transitions from a given initial state to all final states of the residual ion are presented in Figs. 1a -7a :

$$N(^2D) \rightarrow N^+(^3P, {}^1D) \tag{1a}$$

$$N(^2P) \rightarrow N^+(^3P, {}^1D, {}^1S) \tag{2a}$$

$$O(^1D) \rightarrow O^+(^2D, {}^2P) \tag{3a}$$

$$O(^1S) \rightarrow O^+(^2P) \tag{4a}$$

$$C(^1D) \rightarrow C^+(^2P) \tag{5a}$$

$$C(^1S) \rightarrow C^+(^2P) \tag{6a}$$

$$C(^3P) \rightarrow C^+(^2P) \tag{7a}$$

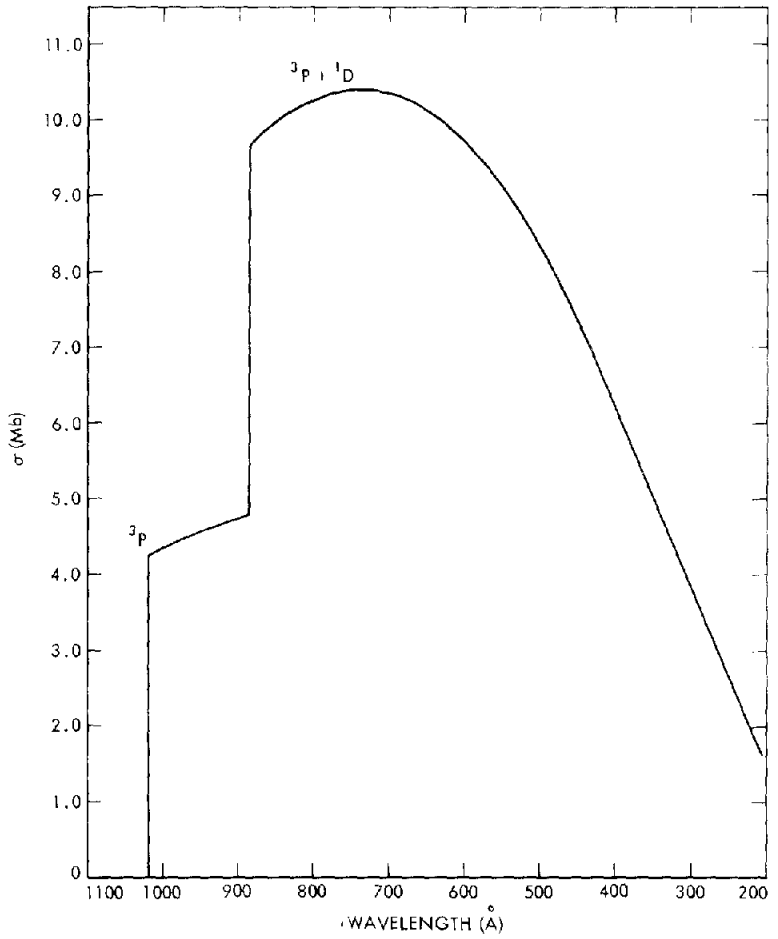

FIG. 1a. Photoionization cross section of nitrogen for the sum of the transitions (1a).

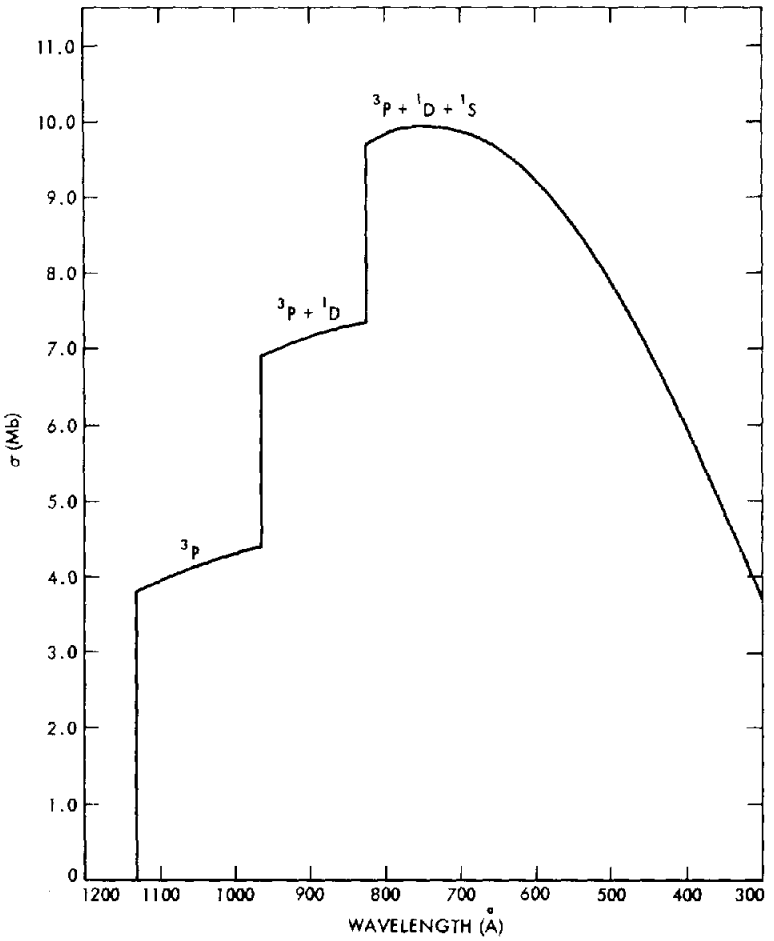

FIG. 2a. Photoionization cross section of nitrogen for the sum of the transitions (2a).

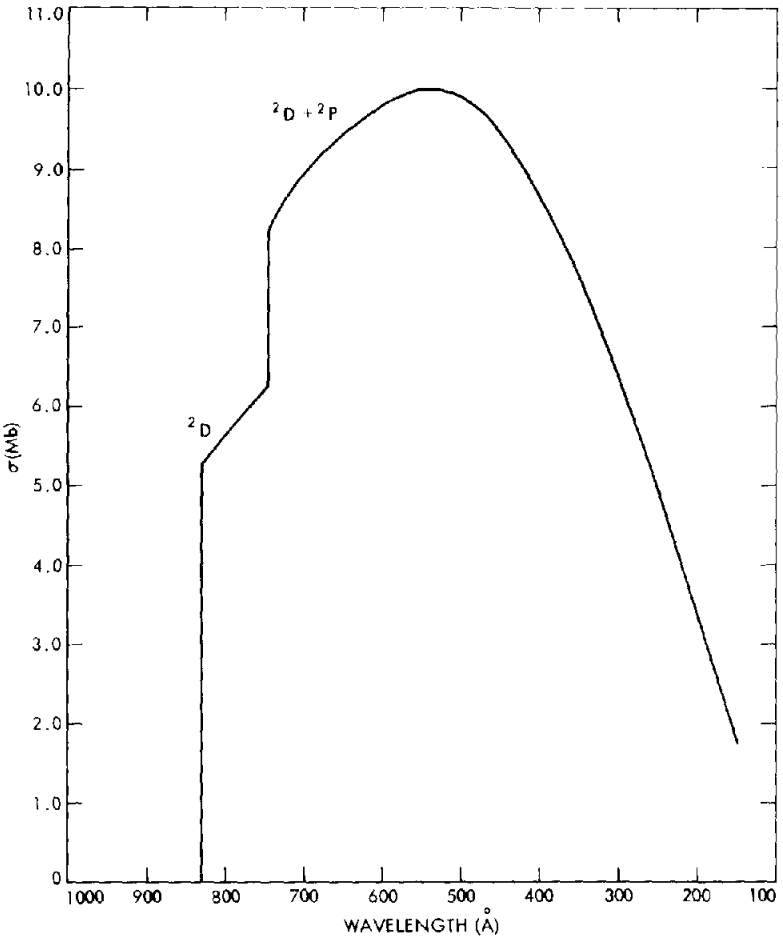

FIG. 3a. Photoionization cross section of oxygen for the sum of the transitions (3a).

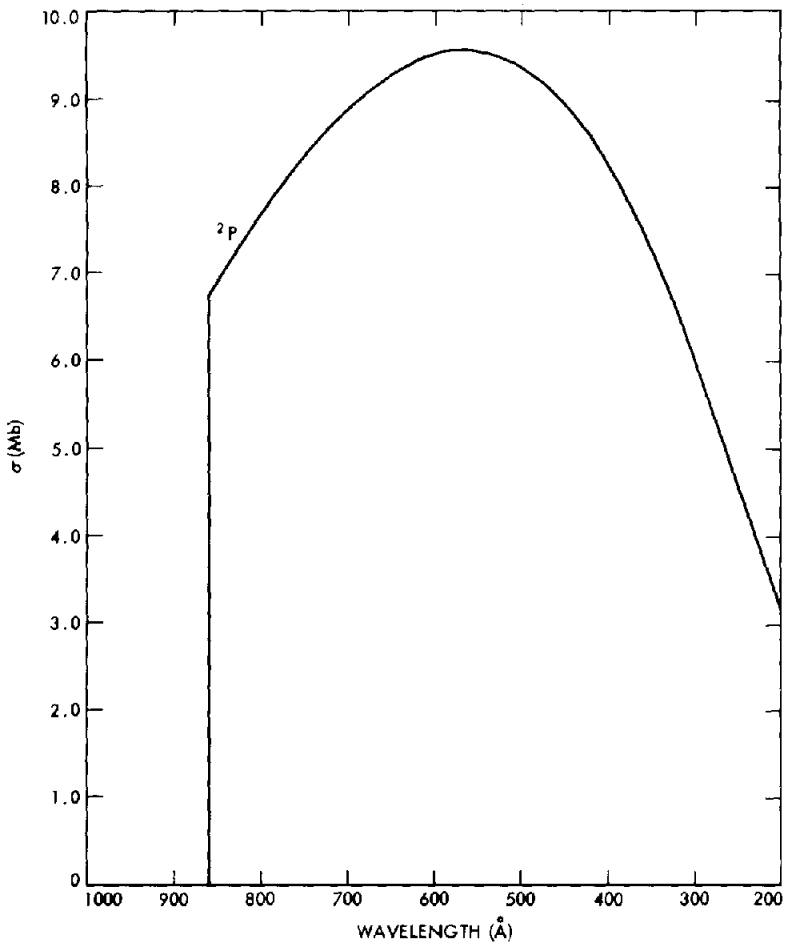

FIG. 4a. Photoionization cross section of oxygen for the transition (4a).

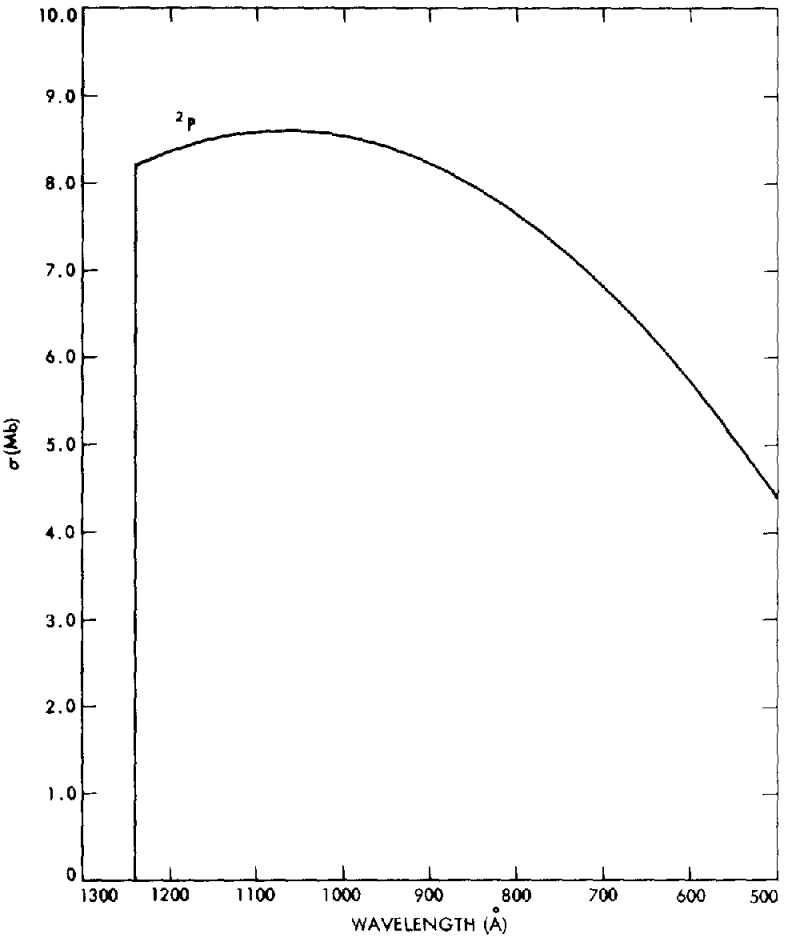

FIG. 5a. Photoionization cross section of carbon for the transition (5a).

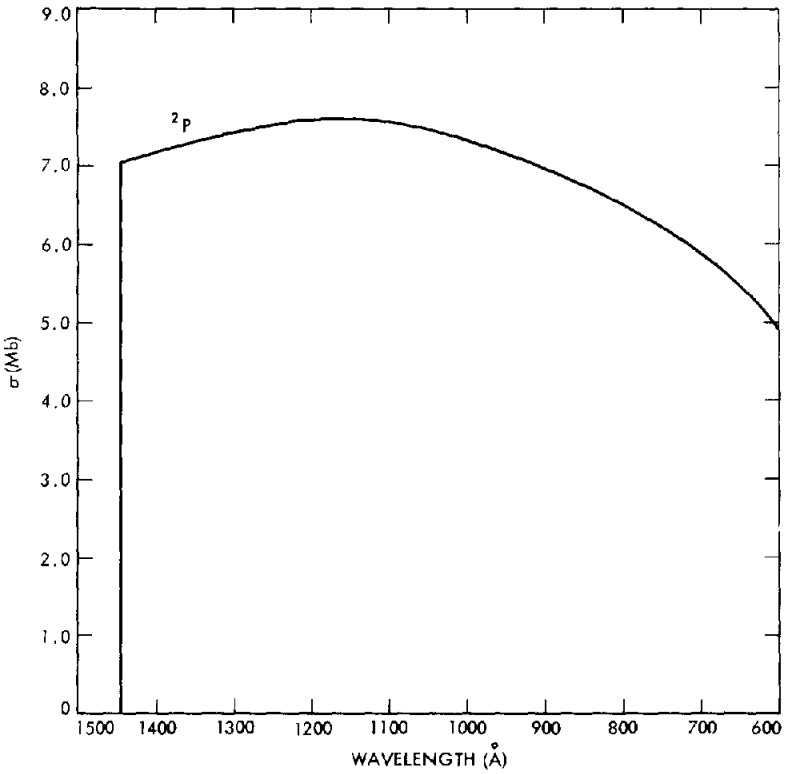

FIG. 6a. Photoionization cross section of carbon for the transition (6a).

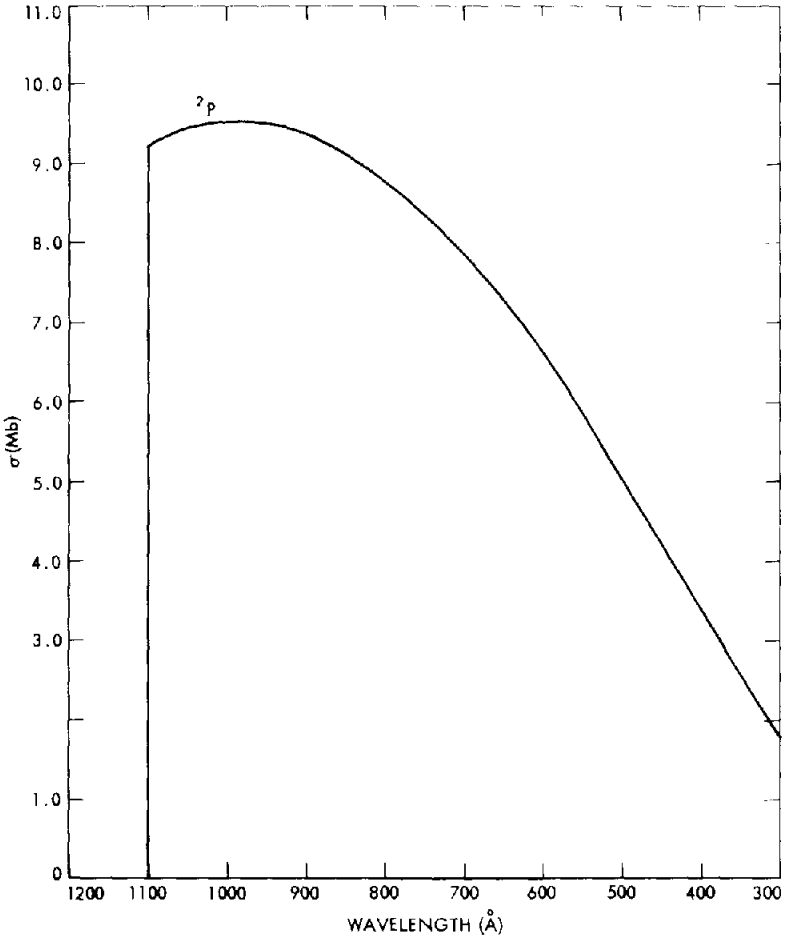

FIG. 7a. Photoionization cross section of carbon for the transition (7a).